HHS Public Access

Author manuscript

J Mol Biol. Author manuscript; available in PMC 2018 February 07.

Published in final edited form as:

J Mol Biol. 2016 April 24; 428(8): 1493–1505. doi:10.1016/j.jmb.2016.02.032.

Induced structural disorder as a molecular mechanism for enzyme dysfunction in phosphoglucomutase 1 deficiency

Kyle M. Stiers[a], **Bailee N. Kain**[a], **Abigail C. Graham**[a], and **Lesa J. Beamer**[a,*]

[a]Biochemistry Department, 117 Schweitzer Hall, University of Missouri, Columbia, MO 65211

Abstract

Human phosphoglucomutase 1 (PGM1) plays a central role in cellular glucose homeostasis, mediating the switch between glycolysis and gluconeogenesis through the conversion of glucose 1-phosphate and glucose 6-phosphate. Recent clinical studies have identified mutations in this enzyme as the cause of PGM1 deficiency, an inborn error of metabolism classified as both a glycogen storage disease and a congenital disorder of glycosylation. Reported here are the first crystal structures of two disease-related missense variants of PGM1, along with the structure of the wild-type enzyme. Two independent glycine to arginine substitutions (G121R and G291R), both affecting key active site loops of PGM1, are found to induce regions of structural disorder, as evidenced by a nearly complete loss of electron density for as many as 23 amino acids. The disordered regions are not contiguous in sequence to the site of mutation, and even cross domain boundaries. Other structural rearrangements include changes in the conformations of loops and side chains, some of which occur nearly 20 Å away from the site of mutation. The induced structural disorder is correlated with increased sensitivity to proteolysis and lower resolution diffraction, particularly for the G291R variant. Examination of the multi-domain effects of these G→R mutations establishes a correlation between interdomain interfaces of the enzyme and missense variants of PGM1 associated with disease. These crystal structures provide the first insights into the structural basis of enzyme dysfunction in PGM1 deficiency, and highlight a growing role for biophysical characterization of proteins in the field of precision medicine.

Introduction

The enzyme PGM1 is well known for its central role in human metabolism, where it mediates the switch between glycolysis and gluconeogenesis. It catalyzes the interconversion of glucose 1-phosphate and glucose 6-phosphate, which also serve as precursors for the nucleotide sugar, galactose, and pentose phosphate pathways. In 2014, a landmark study identified PGM1 deficiency as a hereditary genetic disorder, with characteristics of both a glycogen storage disease (GSDXIV, MIM 612934) and a congenital disorder of glycosylation (CDG) of types I and II [1]. Affected individuals show varying clinical phenotypes, including hepatopathy, dilated cardiomyopathy, hypoglycemia, muscle weakness, exercise intolerance, growth retardation, and congenital malformations of the head such as cleft palate. PGM1 deficiency is autosomal recessive in inheritance, and

*Corresponding author: Lesa J. Beamer, Biochemistry Department, 117 Schweitzer Hall, University of Missouri, Columbia, MO 65211, Office: 573-882-6072, Fax: 573-884-4812, beamerl@missouri.edu.

associated with various types of mutations, including frame shifts, aberrant splicing, and missense variants. To date, the number of affected patients identified is small (~35) but growing [1–7]. Due to the recent characterization of this inherited condition, a biochemical understanding of the disease is not complete, and many questions remain regarding patient prognosis and possible treatments [8].

PGM1 is a cytoplasmic protein with 562 amino acids and is expressed in many human tissues. It belongs to the ubiquitous α-D-phosphohexomutase superfamily, members of which are found in organisms from all kingdoms of life [9]. The catalytic mechanism of phosphoglucomutase from rabbit (97% sequence identity to human) was extensively characterized over several decades by Ray and coworkers ([10] and references therein), who proposed the scheme shown in Fig. 1. The reaction entails two consecutive phosphoryl transfers and proceeds via a bisphosphorylated intermediate. The first phosphoryl transfer takes place from a conserved phosphoserine residue (Ser117) to substrate, creating glucose 1,6-bisphosphate. The intermediate reorients in the active site, and the second phosphoryl transfer occurs from the intermediate back to the protein, creating product and regenerating the active (phosphorylated) version of the enzyme. The reaction is highly reversible, facilitating the role of the enzyme as a metabolic switch.

The identification of PGM1 deficiency as an inherited disease provides new opportunities for understanding this critical human enzyme and its role in metabolism. A number of disease-related missense variants have been biochemically characterized, showing effects on key regions/residues with proposed roles in enzyme function [11]. To date, however, no structural information is available for these mutants, leaving open questions regarding the nature and extent of their impact on protein structure. Here, we address this for the first time by solving crystal structures of two missense variants of PGM1, both of which contain a single Gly→Arg substitution. Previous work had shown that recombinant versions of these proteins, G121R and G291R, are well behaved in solution, but have significant catalytic defects [11]. Through comparison with the high-resolution crystal structure of wild-type (WT) human PGM1, also reported here, we find that both mutant enzymes suffer from regions of induced structural disorder and other effects resulting from the dramatic change in physicochemical characteristics at the site of mutation. The structural impacts of the mutation include both local and longer-range (i.e., >10 Å away) effects, and in some cases extend across domain boundaries. We also establish a correlation between the location of other known missense variants and interdomain interfaces of PGM1. These studies provide the first insights into the molecular origin of enzyme dysfunction responsible for PGM1 deficiency, and may have relevance for future *in vivo* and clinical studies of this inborn error of metabolism.

Results

Overview of the wild-type structure

The high-resolution structure of human WT PGM1 is reported here for the first time. Previous models of human PGM1 relied on the known structure of the rabbit enzyme, which has been refined to a nominal resolution of 2.4 Å (PDB code: 3PMG) [12]. Our 1.85 Å structure (Table 1 and Materials and Methods) confirms many of the features of this model,

but provides additional detail on inter-residue interactions, as well as solvent and sulfate binding sites. We first describe the overall structure of the enzyme, and then the context of the glycines affected by the disease-related mutations G121R and G291R. Although the two copies of the polypeptide chain found in the asymmetric unit are chemically identical, chain A is more highly ordered in the crystals, and is used as the reference in structural descriptions below, unless otherwise noted.

Human PGM1 is a monomeric protein that shares the four-domain architecture common to all enzymes in the α-D-phosphohexomutase superfamily [9]. Its four domains are of roughly equal size, and arranged in an overall heart-shape (Fig. 2a). As noted in the structure of rabbit PGM [13], domains 1–3 share a common mixed α/β core, with a central 4-stranded β-sheet flanked on each side by an α-helix. The active site of PGM1 is located in a large central cleft, formed at the confluence of its four structural domains. This cleft has a molecular surface area of 1670 $Å^2$ as calculated by CASTp [14], and involves 64 residues. It is quite hydrophilic, with nearly 70% of residues being charged or polar (including 11 arginines and lysines), as would be expected for binding of the phosphosugar substrates.

Proposed functional roles of four critical loops within the active site of PGM1 have been previously described (for detailed review see [15]). These loops are from domains 1–4 (D1-D4), respectively, and contain: i) phosphoserine 117 that participates in phosphoryl transfer; ii) the metal-binding loop including the three coordinating aspartates (residues 290, 292 and 294); iii) a sugar-binding loop; and iv) the phosphate-binding site that interacts with the phosphate group of the substrates. Fig. 2b shows a close-up view of these regions in the active site of PGM1; their context in the structure is described below.

Loops i and ii—The phosphoserine and metal binding loops in D1 and D2 are found in close proximity to one another, as required for their joint function in catalysis: Mg^{2+} serves as an electron-withdrawing group to facilitate phosphoryl transfer from phosphoserine 117 (Fig. 1). Phosphoserine 117 resides within a highly conserved TASHNP sequence motif (residues 115–120), and forms an Ω loop that is partially exposed to solvent. Ser117 is found in its dephosphorylated state in the crystal structure, and its side chain Oγ provides one ligand to the bound Mg^{2+} ion. The metal ion is coordinated in octahedral geometry: in addition to Ser117, ligands include three aspartates (residues 288, 290, and 292) and two water molecules. Other nearby residues with proposed roles in phosphoryl transfer include Arg23, which is strictly conserved in the enzyme superfamily, and a potential candidate for the general acid in the reaction [16]. Lys389 is a candidate for the general base: it is analogous to Lys409 of *S. typhimurium* PGM, which when mutated to alanine shows a 3000-fold reduction in k_{cat} [16].

Loop iii—Residues in this loop of D3 are proposed to make key contacts with the O3 and O4 hydroxyl groups of the phosphosugar substrates. The GEESF motif (residues 375–379) is highly conserved in phosphoglucomutases [17], with both Glu376 and Ser378 of human PGM1 proposed to make direct interactions with the O3 and O4 sugar hydroxyls (see model of ligand in Fig. 2b). These residues are precisely oriented such that they can contact the hydroxyl groups of either glucose 1-phosphate or glucose 6-phosphate, which bind in two different orientations in the active site [18]. This dual-binding mode is essential to the

reversibility of the PGM1 reaction, allowing it to use either glucose 1-phosphate or glucose 6-phosphate as substrate.

Loop iv—This region contains residues from two β-strands and a loop in D4 that are proposed to interact with the phosphate group of the substrate/product when bound in the active site. In the crystal structures of WT enzyme and both mutants, a sulfate ion derived from the crystallization buffer is found in this location (Fig. 2b). This sulfate acts as structural mimic for the phosphate group of the substrate, and confirms the identity of key residues involved in direct phosphate contacts, including the side chains of Arg503, Ser505, and Arg515, as well as the backbone amide of Gly506. Several residues in this loop (507–509) are missing from the electron density maps, suggesting they are mobile. This would be consistent with motion of the loop during the catalytic cycle, whereby it closes upon substrate binding and opens to release product.

Context of glycines 121 and 291 in the WT structure

Gly121 is located immediately following loop (i), just after the highly conserved TASHNP motif. In the WT structure, Gly121 is in a partially buried region between two turns, and has ϕ/ψ angles of ~130/175°, which are uncommon except for glycine. Gly121 makes no direct contacts to other residues, but is located at the interface between D1 and D2 of the protein (Fig. 2b), adjacent to a short helix (residues 257–259) and extended region (residues 260–269) in D2.

Gly291 is found within loop (ii), the metal binding loop of PGM1. This loop is deeply buried within the active site cleft, and adjacent to residues from both D1 and D3 (Fig. 2b). Gly291 is the intervening residue between Asp290 and Asp292, both of which coordinate the metal ion. Its ϕ/ψ angles are ~80/10°, values preferred for glycine. Gly291 makes several interactions with other residues, including a hydrogen bond between its backbone amide proton and the side chain of Asp288, and two hydrogen bonds from its backbone carbonyl to the amide of Gly391 and a water-mediated interaction to the backbone amide of Leu393.

Structure of the G121R missense variant

The crystal structure of the G121R missense variant was determined to 2.35 Å (Table 1; Materials and Methods). Fig. 3a,b show an overview of the structure of the mutant, superimposed with that of WT enzyme. While the two structures are quite similar with an overall root-mean-square-deviation (rmsd) of 0.51 Å for 540 C_α pairs), the mutation produces both local and longer-range structural changes in the enzyme. In the vicinity of residue 121, the introduced arginine displaces the side chain of a nearby residue, Phe257, which packs in the interface between D1 and D2 in the WT structure (Fig. 3c). In its place, Arg121 makes adventitious hydrogen bond interactions with the backbone carbonyls of Leu254 and Asp62 (Fig. 3d). These fortuitous interactions appear to compensate for the introduction of the polar, positively charged side chain of the arginine, which would otherwise be unfavorable in this buried environment. Despite the proximity of the G121R mutant to active site loops (i) and (ii), few changes to this region are observed, at least in chain A in the crystal structure. In chain B, which is less well ordered, neither the side chain of Arg121 nor loop (i) is clearly observed.

In addition to this local structural rearrangement, longer-range changes also occur, particularly in the adjacent region of D2. Electron density for the displaced side chain of Phe257 cannot be located in the maps, and subsequent to this residue, density for the entire polypeptide chain disappears and does not clearly reappear until approximately residue 265, presumably due to dynamic disorder in the crystal. A comparison of this area in the G121R and WT enzyme structures is shown in Fig. 3c. Although these residues have limited regular secondary structure in the WT enzyme, a number of well-defined inter-residue interactions involving this region are evident, all of which are lost in the structure of the mutant. The induced structural disorder appears to originate from the steric rearrangement of Phe257 forced by the arginine substitution, and subsequent accommodation of its side chain in the D1-D2 interface. Despite the extended region of disorder in the middle of the sequence, the polypeptide chain eventually returns to its proper course, adopting an essentially WT fold following residue 270. In total, the propagated effects of the G121R substitution extend more than 17 Å from the site of the mutation, with induced disorder of seven amino acids (Table 2).

Structure of the G291R missense variant

The crystal structure of the G291R missense variant was determined to 2.75 Å (Table 1; Materials and Methods). Despite crystals of similar size, diffraction data collected from these crystals were noticeably lower in resolution compared to WT (1.85 Å) and the G121R mutant (2.5 Å). The structure of the G291R missense variant superimposed with that of WT enzyme is shown in Fig. 4a,b. As is the case for G121R, the overall structure of G291R is quite similar to that of WT (C_α rmsd of 0.83 Å for 525 residues). Nevertheless, the single arginine substitution causes widespread structural changes, including induced disorder in three loops near the active site, as well as conformational rearrangements and differences in residue packing (Fig. 4c), as detailed below.

In the G291R structure, loop (ii) shows changes in the conformation of both its polypeptide backbone and side chains. The corresponding areas of the WT and G291R structures are displayed in Fig. 4d,e. The backbone angles of the polypeptide chain of G291R have altered to accommodate the introduced arginine side chain and the less flexible backbone of this residue relative to glycine, moving the loop to a more solvent-exposed position in the active site cleft. Accompanying the backbone changes are significant differences in the orientations of the three metal-coordinating aspartates, with concomitant destruction of the metal-binding site. Aspartates 290 and 292, in particular, reorient dramatically: Asp290 becomes fully solvent exposed, while Asp292 makes a novel hydrogen bond interaction with Thr93 (Fig. 4e). The introduced arginine side chain is apparent in the electron density maps of chain A, where it points directly toward the center of the positively charged active site cleft. This unfavorable electrostatic environment may be mitigated by interactions with a sulfate ion and the high pH of the crystals (see Materials and Methods), which would tend to deprotonate Arg291 and/or other nearby positive residues.

Another apparent outcome of the conformational rearrangement of loop (ii) is induced disorder in the phosphoserine loop (i) of D1. As can be seen by comparing Fig. 4d and e, the native conformation of this loop would be in steric conflict with the rearranged position of

loop (ii) in the mutant. Consequently, residues 117–125 are disordered in the electron density maps of the G291R mutant. In an apparent series of propagated changes, several other nearby loops are also disordered, including another in D1 (residues 64–65) and a larger region in D2 (residues 256–267). In total, 23 residues in two domains are affected by induced disorder in the structure of G291R mutant (Table 2), including some that are nearly 20 Å away from the site of the mutation. Other structural effects include changes in the packing of residues, such as Trp359 (Fig. 4c), which is one of several residues near loop (ii) that appear to have adjusted in response to its rearranged conformation. Thus, while the overall structure of the enzyme remains largely intact, changes due to this single residue substitution propagate across the protein, affecting multiple residues and domains.

Correlation between structural and biochemical data

The crystal structures of the G121R and G291R missense variants provide a valuable opportunity for understanding biochemical data on these disease-related mutants [11]. Previous work on G121R showed that this protein is well expressed in *E. coli*, soluble, and its apparent molecular weight in solution is similar to WT enzyme. Likewise, its near-UV circular dichroism spectrum and T_m (only 1° lower) are quite similar to those of WT, although its interaction with the fluorescent dye 1-anilinonaphthalene-8-sulfonic acid (ANS) shows a moderate increase. Its catalytic activity is nevertheless significantly compromised, with k_{cat} / K_m only 0.4% of WT (Table 2), although Ser117 in the mutant protein can still be phosphorylated by the activator glucose 1,6-bisphosphate. The structural studies of this variant, showing various perturbations near the active site cleft, are consistent with its catalytic impairment, which is significant but not complete. At least in chain A of the crystal structure, the position of Ser117 and the metal-binding loop are quite similar to WT, implying the mutant should be competent for catalysis. Disorder of loop (i) in chain B of the crystals, however, suggests that the mutant protein may exist as an inactive conformer more frequently than the WT enzyme. Together with other effects, including many small changes in/near the active site environment due to the disordered regions, it is not difficult to rationalize an overall decrease in the catalytic efficiency of G121R.

In the case of G291R, the structural disruption is more extensive, and this is reflected in the extreme catalytic defect of this mutant, which is the most impaired of all the PGM1 missense variants characterized to date (activity below detection in *in vitro* kinetic assays; Table 2) [11]. The inactivity of G291R is consistent with structural effects of the mutation on key loops within the active site, perturbing both metal binding and phosphoryl transfer, two essential features of the reaction. Defects in these processes are also reflected by the inability of the G291R variant to be phosphorylated under the conditions tested. While not directly linked to catalysis, the disordered loop containing residues 64–65 disrupts a conserved salt-bridge between Asp62 and Arg64, which in turn makes multiple interactions with loop (i) in the WT structure. Absence of these anchoring interactions with the critical phosphoserine loop would be a further impediment to phosphoryl transfer by this mutant protein.

The structural effects of the G291R missense variant are also interesting to consider in light of other biochemical data on this protein [11]. The mutant is generally well expressed in *E.*

coli and soluble, although not quite at WT levels. In solution, the purified protein is well behaved with a similar apparent molecular weight to WT enzyme, while its T_m is a bit lower (~3°). Notably, however, its binding to ANS is significantly increased, and the G291R mutant is also more susceptible to limited proteolysis. These results make sense based on the observed changes in the crystal structure, particularly the regions of induced disorder, which could be easily proteolyzed. Similarly, the perturbation of the 3-way domain interface in which this residue is involved, and concomitant changes in residue packing (Fig. 4c), can be easily envisioned to allow enhanced binding of ANS, which typically occurs in apolar crevices in protein structures [19]. In the future, it may be informative to conduct studies such as ANS-binding and limited proteolysis in the presence and absence of ligand, to determine whether ligand binding can mitigate the disordered regions of structure in mutants such as G121R and G291R.

Missense variants of PGM1 cluster in domain-domain interfaces

In light of the multi-domain effects of the G121R and G291R mutants, we analyzed other disease-related missense variants of PGM1 relative to the interdomain interfaces of the protein. The conserved four-domain architecture of PGM1 and the location of the active site cleft at the juncture of these structural domains (Fig. 2A) imply that mutations in these regions could be disproportionately disruptive to enzyme function. Moreover, in addition to the 13 originally characterized [11], several new missense mutants of PGM1 associated with disease have recently been identified [6]. These include G230E, T337M, P336R, R422W, R503Q, and R515L (Fig. 5). It can be seen that these new variants expand the structural regions associated with enzyme dysfunction: while many are near the active site cleft, others, such as G230E and R422W, are more distant from known regions of functional importance.

To assess the potential correlation between domain interfaces and the pathogenicity of missense variants, residues in the structure of WT PGM1 involved in each possible domain-domain interface were identified using LigPlot+ [20] and are detailed in Supplementary Fig. S1. Of the six potential interfaces, four have contacting residues in the crystal structure: D1-D2, D1-D3, D2-D3, and D3-D4. Each interface includes at least one known disease-related mutation, although most are in either the D1-D2 or D3-D4 interface (see following paragraph). Notably, only one of the known missense variants resides in two distinct domain interfaces: G291R, which contacts residues in D1, D2, and D3 (see also Fig. 4c). Although not affected by known mutations, 13 other residues in PGM1 are also involved in 3-way domain interactions (Supplementary Fig. S1) and might also be expected to be especially sensitive to structural perturbation by mutation.

As many of the known missense mutations localize to the D1-D2 and D3-D4 interfaces, it is convenient to consider domains 2 and 3 (residues 192–421) as a single structural unit (D2/3), and the interface between this unit and the rest of the enzyme as a single, extended surface (blue in Fig. 5). This large interface contains 101 residues out of 562 in the protein (18%), including much of the active site cleft, but also extends to include regions between D1-D2 and D3-D4 that are relatively far from the catalytic center. Using this convention, it can be seen that the interface with the D2/3 unit encompasses 11 of the 18 residues affected by

missense variants of PGM1, while four others are immediately adjacent (a combined total of 83%). Thus it appears that mutations in this interface account for a striking proportion of the currently recognized disease-related variants of PGM1. It remains to be seen whether this distribution will change as new missense mutants are identified.

In addition to G121R and G291R, these interdomain mutations include many previously categorized as deleterious to catalysis (D62H, T115A, G121R, G230E, D263G/Y, G291R, T337M, and R503Q) [6,11]. However, several also appear to cause folding problems (P336R, E377K, E388K, and R422W) [6,11]. This suggests that a gradation of effects can occur due to substitutions at this interdomain interface, with the functional outcome dependent on factors such as the physicochemical change of the mutation and the structural interactions of the WT residue. It should be noted that several missense variants of PGM1 fall well outside of the D2/3 interface, suggesting the presence of additional “residue clusters” (e.g., residues 38 and 41, Fig. 5) with distinct functional roles, perhaps in protein folding. Mutants affecting residue 38 and 41 also tend to have milder clinical phenotypes than those affecting the interface residues [6], although the heterozygous backgrounds and limited number of patients prohibits a definitive analysis.

DISCUSSION

Missense mutations are the most common genetic variation associated with monogenic disease, with >70,000 examples currently found in the Human Gene Mutation Database [21]. Decreased stability and folding problems are estimated to account for the pathogenicity of more than two-thirds of these [22,23], resulting in problems such as aggregation, improper trafficking, and rapid degradation. Less frequently, missense mutants are identified that directly impact function, i.e., affecting key catalytic residues or causing discrete structural changes like disruption of hydrogen bonding networks. While biochemical studies have been conducted on hundreds of missense variants responsible for human disease, parallel structural studies are not nearly as common, particularly for mutants with effects on protein folding/stability. Hence, while the importance of missense variants in human disease is well appreciated, a molecular understanding of the results of the mutation is often elusive [24], with many studies relying on modeling or other computational methods to predict likely effects.

Here we provide direct structural insights into the molecular basis of enzyme dysfunction for two Gly→ Arg missense mutations associated with PGM1 deficiency. The structural studies of these two variants reveal multiple changes as a result of the single amino acid substitution, including the complete loss of previously ordered regions of the polypeptide chain. In lieu of structural information, biochemical data on the G121R and G291R variants suggested they be categorized as a “catalytic mutants” rather than defective in protein folding. The crystallographic studies reveal that induced structural disorder affecting key residues in/near the active site is likely involved in this catalytic impairment, along with other structural changes such as conformational rearrangements. In essence, this blends the two previously suggested categories of enzyme dysfunction [11], suggesting that small regions of disordered structure may be one source of catalytic defects in missense variants of PGM1.

The G→R substitution in the G121R and G291R mutants is one of the more dramatic physicochemical changes among the disease-related variants of PGM1 [15], and is also one of the two variants most frequently associated with human disease in general [25,26]. Given the obvious differences between glycine and arginine, structural repercussions on the enzyme are not unexpected. Indeed, it may be more surprising that the overall tertiary fold of PGM1 remains largely intact, despite the structural impacts of the mutation. It appears that the structural scaffold of PGM1 has a high threshold of robustness, i.e., an excess of stability that buffers the destabilizing effects of mutations [23], which may be a testimony to the long evolutionary history of phosphoglucomutases. Also, as established in other systems [27], the multi-domain architecture of the enzyme could offer advantages, allowing individual domains “fold up” around the site(s) of structural disruption, despite their internal locations in the polypeptide chain. For several related proteins ([28,29] and PDB code: 1WJW), isolated versions of D4 fold correctly, supporting the notion of independent domain folding in this enzyme superfamily.

As is true for many enzymes, the active site of PGM1 is formed at the juncture of its structural domains, and this cleft includes many of the known disease-related mutants. However, by considering the D2/3 interface, a larger area of high mutational density is defined, that includes several additional missense variants. This perspective appears to connect disparate structural regions of PGM1 with the observed pathogenic effects of the mutations, and thus may have potential utility for predicting clinical phenotypes as new missense variants of PGM1 are identified. Moreover, we expect this theme could be relevant to many human diseases, given the preponderance of multi-domain proteins in the proteomes of higher organisms [30]. Several other proteins involved in inherited disorders also have missense variants that localize to interdomain interfaces [31–33], although their distribution across the 3D-structure is much wider overall, perhaps due to the larger number of mutations identified.

By combining the insights gained from the crystal structures of PGM1 with previous biochemical data [11], it is possible to assess, in retrospect, the utility of various assays used to characterize these mutant proteins. On one hand, assays monitoring global changes in protein behavior, like circular dichroism or dynamic light scattering, were not informative, at least with regard to the presence of induced structural disorder. On the other hand, methods such as the binding of ANS and limited proteolysis, appear to correlate well with the structural data. Accordingly, we can propose that several other disease-related PGM1 mutants may also suffer from induced structural disorder. This would include D62H and T115A, two mutants with profiles that fall between those of G121R and G291R in ANS-binding spectra [11]. In contrast, other missense mutants, such as D263Y and T19A, show little change from WT enzyme in this assay, suggesting that their defects discretely affect catalysis/ligand binding, rather than protein structure. As many other proteins have missense variants that show differences in such assays (e.g., [34–36]), it is possible that induced disorder is a common outcome of disease-related mutations, which is underappreciated due to lack of structural information.

Overall, it seems that a combination of structural, kinetic, and other biochemical assays should be considered to fully describe the biochemical phenotype of the PGM1 missense

variants. These characterizations may help direct and interpret future *in vivo* studies. For example, it will be intriguing to see whether "slightly misfolded" variants of PGM1, such as G121R and G291R, are targeted for degradation by the proteasome in human cells. Such studies have not yet been conducted, but if this turns out to be the case, use of these assays on newly identified variants might help suggest patients who would benefit from treatment with proteasome inhibitors. Proteostasis regulators have proven useful in the treatment of other inherited diseases associated with variants that affect protein folding and or stability [37].

Due to the recent recognition of PGM1 deficiency in the clinical literature, and the mild phenotypes of some patients, the number of individuals confirmed with this disorder is still quite small. To date, only one person with the G121R mutation in PGM1 has been identified, who was homozygous for the mutation and deceased at age 8 with end stage dilated cardiomyopathy [1]. In the case of G291R, two unrelated patients are known, both heterozygous for other mutations in PGM1 (either a nonsense or different missense mutant), and who have mild-moderate phenotypes [1,2,6]. Our structural studies therefore represent "personalized" crystal structures, a new tool in the growing field of precision medicine [38,39]. Such structures are likely to have a growing role in the understanding and treatment of inherited disease. In the case of PGM1 deficiency, structural studies may be especially relevant given difficulties in correlating *in vitro* enzyme activity with patient phenotype [6]. Additional crystal structures of other missense variants PGM1 will likely provide further insights into the molecular bases of enzyme dysfunction. In combination with future clinical and *in vivo* studies, this should help unravel the multiple patient phenotypes associated with PGM1 deficiency.

Material and Methods

Protein expression, purification, and crystallization

Human WT PGM1 and the G121R and G291R missense variants were expressed recombinantly in *E. coli* and purified to homogeneity via an N-terminal histidine tag, as previously described [11]. Prior to crystallization, the histidine tag was removed by cleavage with tobacco etch virus (TEV) protease as follows. Proteins were dialyzed into Buffer 1 (0.3 M NaCl and 50 mM Tris, pH 8.0), then mixed at 10–20 fold ratio (w/w) with TEV protease (Buffer 1 with 0.5 mM DTT and 0.5 mM EDTA) and glycerol (10% v/v final). The mixture was incubated at room temperature for 3–4 hours, kept overnight at 4° C, and extensively dialyzed into Buffer 1 before loading onto a pre-equilibrated Ni-NTA column. Cleaved protein eluted in the flow through; TEV and any residual His-tagged proteins were retained on the column, and eluted with Buffer 1 plus 300 mM imidazole, pH 8.0. Successful cleavage was confirmed by electrospray ionization mass spectrometry; all proteins were the expected molecular weight with no indication of proteolysis. The purified, cleaved proteins were dialyzed into a solution of 50 mM MOPS, pH 7.4, with 1 mM $MgCl_2$, and concentrated to ~10 mg / mL or higher. If not used immediately, samples were flash-frozen in liquid nitrogen and stored at −80° C. Prior to crystallization, the protein was diluted as desired and 0.22 μm filtered.

Initial crystallization screens were set up with Crystal Screen kits 1 and 2 (Hampton Research) and Wizard screen kits 1 and 2 (Emerald BioSystems Inc.) at protein concentrations ranging from 10–18 mg / mL using the hanging drop vapor diffusion method at 20° C. Drops containing 2 μl protein solution and 2 μl crystallization buffer were sealed over a 0.5 mL reservoir. The WT protein crystallized successfully in a range of conditions from ammonium or lithium sulfate (1.35 – 1.85 M) with either 0.1 M buffer of MES, pH 6.0, or Tris HCl, pH 7.5 – 8.5. Crystals grew in approximately one week. The G121R mutant crystallized in ~1.5 M ammonium sulfate with lithium sulfate (0.12–0.18 M) and 0.1 M CAPS, pH 10.5. The G291R mutant crystallized in ~1.0 M sodium citrate with 0.1 M CHES buffer, pH 9.7.

All crystals were cryoprotected using a solution of well buffer supplemented with 30% glycerol (v/v), mounted on Hampton loops, and flash cooled in liquid nitrogen. WT and mutant proteins crystallized in space group $P4_12_12$ with ~60% solvent ($\mathbf{V}_M$ = 3.04 Å^3/Da). The asymmetric unit contains two copies of the polypeptide chain.

X-ray Diffraction Data Collection and Refinement

Diffraction data were collected at a wavelength of 1.00003 Å from single crystals on beamline 4.2.2 of the Advanced Light Source using a Taurus-1 CMOS detector in shutterless mode. The data were processed using XDS [40] and AIMLESS [41] via CCP4i [42]. Data processing statistics are listed in Table 1. Values of $CC_{1/2} > 0.30$ [43] and R_{pim} [44] were considered when determining the high resolution cutoff, due to the large number of images (1800–3600 per data set) and high redundancy obtained with the shutterless data collection. In addition, all data sets were anisotropic, especially those of G121R and G291R, which contributes to poor R_{merge} statistics at high resolution for these two data sets, although $CC_{1/2}$ is acceptable in the chosen range.

Crystallographic refinement calculations for the WT enzyme were initiated using coordinates derived from the 2.4 Å resolution structure of rabbit PGM (PDB code: 3PMG), which crystallizes isomorphously with human PGM1 (97% sequence identity). Refinement was performed with REMAC 5.0 [45] and PHENIX [46]; progress was monitored by following R_{free} with 5% of each data set was set aside for cross validation. The B-factor model consisted of an isotropic B-factor for each atom; TLS refinement was used as automated in PHENIX. COOT [47] was used for model building. Additional details of the refinement are on Table 1. The structures of the G121R and G291R missense variants were determined using the model of WT enzyme, starting with molecular replacement using MOLREP [48] or rigid-body followed by restrained refinement. The R_{free} data sets for both mutants were constrained to match those of the WT data. The structures were validated using MolProbity [49]. Refinement statistics are listed in Table 1. Structural figures were prepared with PYMOL [50]. Coordinates and structure factor amplitudes have been deposited in the PDB under the accession numbers listed in Table 1.

Supplementary Material

Refer to Web version on PubMed Central for supplementary material.

Acknowledgments

We thank Jay Nix of ALS beamline 4.2.2 for assistance with data collection and processing, Ritcha Mehra-Chaudhary of the University of Missouri Structural Biology Core for assistance with protein purification, and Brian Mooney of the University of Missouri Charles W. Gehrke Proteomics Center for mass spectrometry. This work was supported by grants to LJB from the Patton Trust of the Kansas City Area Life Sciences Research Foundation and the National Science Foundation (MCB-0918389). Part of this work was performed at the Advanced Light Source. The Advanced Light Source is supported by the Director, Office of Science, Office of Basic Energy Sciences, of the U.S. Department of Energy under contract DE-AC02-05CH11231.

Abbreviations not defined in text

CAPS	N-cyclohexyl-3-aminopropanesulfonic acid
CHES	N-Cyclohexyl-2-aminoethanesulfonic acid
DTT	dithiothreitol
EDTA	ethylenediaminetetraacetic acid
MOPS	3-morpholinopropane-1-sulfonic acid
MES	2-(N-morpholino)ethanesulfonic acid
TRIS	2-Amino-2-hydroxymethyl-propane-1,3-diol
PDB	Protein Data Bank

References

1. Tegtmeyer LC, Rust S, van Scherpenzeel M, Ng BG, Losfeld ME, Timal S, et al. Multiple Phenotypes in Phosphoglucomutase 1 Deficiency. N Engl J Med. 2014; 370:533–542. [PubMed: 24499211]
2. Pérez B, Medrano C, Ecay MJ, Ruiz-Sala P, Martínez-Pardo M, Ugarte M, et al. A novel congenital disorder of glycosylation type without central nervous system involvement caused by mutations in the phosphoglucomutase 1 gene. J Inherit Metab Dis. 2012; 36:535–542. [PubMed: 22976764]
3. Timal S, Hoischen A, Lehle L, Adamowicz M, Huijben K, Sykut-Cegielska J, et al. Gene identification in the congenital disorders of glycosylation type I by whole-exome sequencing. Hum Mol Genet. 2012; 21:4151–4161. [PubMed: 22492991]
4. Kucukcongar A, Tumer L, Suheyl Ezgu F, Seher Ksapkara C, Jaeken J, Matthijs G, et al. A case with rare type of congential-disorder of glycosylation: PGM1-CDG. Genet Couns. 2015; 26:87–90. [PubMed: 26043514]
5. Ondruskova N, Honzik T, Vondrackova A, Tesarova M, Zeman J, Hansikova H. Glycogen storage disease-like phenotype with central nervous system involvement in a PGM1-CDG patient. Neuro Endocrinol Lett. 2014; 35:137–141. [PubMed: 24878975]
6. Wong, S., Beamer, LJ., Gadomski, T., Honzik, T., Mohamed, M., Wortmann, SB., et al. Defining the phenotype and assessing severity in Phosphoglucomutase-1 deficiency. Under Revision
7. Loewenthal N, Haim A, Parvari R, Hershkovitz E. Phosphoglucomutase-1 deficiency: Intrafamilial clinical variability and common secondary adrenal insufficiency. Am J Med Genet Part A. 2015; 167:3139–3143.
8. Morava E. Galactose supplementation in phosphoglucomutase-1 deficiency; review and outlook for a novel treatable CDG. Mol Genet Metab. 2014; 112:275–279. [PubMed: 24997537]
9. Shackelford GS, Regni CA, Beamer LJ. Evolutionary trace analysis of the alpha-D-phosphohexomutase superfamily. Protein Sci. 2004; 13:2130–2138. [PubMed: 15238632]

10. Ray WJ, Burgner JW, Post CB. Characterization of vanadate-based transition-state-analogue complexes of phosphoglucomutase by spectral and NMR techniques. Biochemistry. 1990; 29:2770–8. [PubMed: 2140697]
11. Lee Y, Stiers KM, Kain BN, Beamer LJ. Compromised catalysis and potential folding defects in in vitro studies of missense mutants associated with hereditary phosphoglucomutase 1 deficiency. J Biol Chem. 2014; 289:32010–32019. [PubMed: 25288802]
12. Liu Y, Ray WJ, Baranidharan S. Structure of rabbit muscle phosphoglucomutase refined at 2.4 Å resolution. Acta Crystallogr D. 1997; 53:392–405. [PubMed: 15299905]
13. Dai J-B, Ray WJ, Konno M. The crystal structure of muscle phosphoglucomutase refined at 2.7 Å resolution. J Biol Chem. 2001:1–16. [PubMed: 11696554]
14. Dundas J, Ouyang Z, Tseng J, Binkowski A, Turpaz Y, Liang J. CASTp: Computed atlas of surface topography of proteins with structural and topographical mapping of functionally annotated residues. Nucleic Acids Res. 2006; 34:116–118.
15. Beamer LJ. Mutations in hereditary phosphoglucomutase 1 deficiency map to key regions of enzyme structure and function. J Inherit Metab Dis. 2014:1–14. [PubMed: 23653226]
16. Lee Y, Mehra-Chaudhary R, Furdui C, Beamer LJ. Identification of an essential active-site residue in the alpha-D-phosphohexomutase enzyme superfamily. FEBS J. 2013; 280:2622–2632. [PubMed: 23517223]
17. Mehra-Chaudhary R, Mick J, Tanner JJ, Henzl MT, Beamer LJ. Crystal structure of a bacterial phosphoglucomutase, an enzyme involved in the virulence of multiple human pathogens. Proteins. 2011; 79:1215–29. [PubMed: 21246636]
18. Regni C, Naught L, Tipton Pa, Beamer LJ. Structural Basis of Diverse Substrate Recognition by the Enzyme PMM/PGM from P. aeruginosa. Structure. 2004; 12:55–63. [PubMed: 14725765]
19. Hawe A, Sutter M, Jiskoot W. Extrinsic fluorescent dyes as tools for protein characterization. Pharm Res. 2008; 25:1487–99. [PubMed: 18172579]
20. Laskowski RA, Swindells MB. LigPlot+: Multiple ligand-protein interaction diagrams for drug discovery. J Chem Inf Model. 2011; 51:2778–2786. [PubMed: 21919503]
21. Cooper DN, Stenson PD, Chuzhanova Na. The Human Gene Mutation Database (HGMD) and its exploitation in the study of mutational mechanisms. Curr Protoc Bioinformatics. 2006; Chapter 1(Unit 1.13)
22. Yue P, Li Z, Moult J. Loss of Protein Structure Stability as a Major Causative Factor in Monogenic Disease. J Mol Biol. 2005; 353:459–473. DOI: 10.1016/j.jmb.2005.08.020 [PubMed: 16169011]
23. Tokuriki N, Tawfik DS. Stability effects of mutations and protein evolvability. Curr Opin Struct Biol. 2009; 19:596–604. [PubMed: 19765975]
24. Stefl S, Nishi H, Petukh M, Panchenko AR, Alexov E. Molecular Mechanisms of Disease-Causing Missense Mutations. J Mol Biol. 2013; 425:3919–3936. [PubMed: 23871686]
25. Petukh M, Kucukkal TG, Alexov E. On human disease-causing amino acid variants: Statistical study of sequence and structural patterns. Hum Mutat. 2015; 36:524–534. [PubMed: 25689729]
26. Peterson TA, Doughty E, Kann MG. Towards precision medicine: Advances in computational approaches for the analysis of human variants. J Mol Biol. 2013; 425:4047–4063. [PubMed: 23962656]
27. Han J-H, Batey S, Nickson Aa, Teichmann Sa, Clarke J. The folding and evolution of multidomain proteins. Nat Rev Mol Cell Biol. 2007; 8:319–30. [PubMed: 17356578]
28. Schramm AM, Karr D, Mehra-Chaudhary R, Van Doren SR, Furdui CM, Beamer LJ. Breaking the covalent connection: Chain connectivity and the catalytic reaction of PMM/PGM. Protein Sci. 2010; 19:1235–42. [PubMed: 20512975]
29. Wei Y, Marcink TC, Xu J, Sirianni AG, Sarma AVS, Prior SH, et al. Chemical shift assignments of domain 4 from the phosphohexomutase from Pseudomonas aeruginosa suggest that freeing perturbs its coevolved domain interface. Biomol NMR Assign. 2014; 8:329–333. [PubMed: 23893395]
30. Ekman D, Björklund AK, Frey-Skött J, Elofsson A. Multi-domain proteins in the three kingdoms of life: orphan domains and other unassigned regions. J Mol Biol. 2005; 348:231–43. [PubMed: 15808866]

31. Pey AL, Stricher F, Serrano L, Martinez A. Predicted effects of missense mutations on native-state stability account for phenotypic outcome in phenylketonuria, a paradigm of misfolding diseases. Am J Hum Genet. 2007; 81:1006–1024. [PubMed: 17924342]
32. Ohto U, Usui K, Ochi T, Yuki K, Satow Y, Shimizu T. Crystal structure of human β-galactosidase: Structural basis of G M1 gangliosidosis and morquio B diseases. J Biol Chem. 2012; 287:1801–1812. [PubMed: 22128166]
33. Fulop K, Barna L, Symmons O, Zavodsky P, Varadi A. Clustering of disease-causing mutations on the domain-domain interfaces of ABCC6. Biochem Biophys Res Commun. 2009; 379:706–709. [PubMed: 19133228]
34. Bozzi M, Cassetta A, Covaceuszach S, Bigotti MG, Bannister S, Hübner W, et al. The Structure of the T190M Mutant of Murine α-Dystroglycan at High Resolution: Insight into the Molecular Basis of a Primary Dystroglycanopathy. PLoS One. 2015; 10:e0124277. [PubMed: 25932631]
35. Lee MS, Green R, Marsillac SM, Coquelle N, Williams RS, Yeung T, et al. Comprehensive analysis of missense variations in the BRCT domain of BRCA1 by structural and functional assays. Cancer Res. 2010; 70:4880–4890. [PubMed: 20516115]
36. Bjørgo E, Knappskog PM, Martinez A, Stevens RC, Flatmark T. Partial characterization and three-dimensional-structural localization of eight mutations in exon 7 of the human phenylalanine hydroxylase gene associated with phenylketonuria. Eur J Biochem. 1998; 257:1–10. [PubMed: 9799096]
37. Muntau AC, Leandro J, Staudigl M, Mayer F, Gersting SW. Innovative strategies to treat protein misfolding in inborn errors of metabolism: pharmacological chaperones and proteostasis regulators. J Inherit Metab Dis. 2014; 37:505–523. [PubMed: 24687294]
38. Kroncke BM, Vanoye CG, Meiler J, George AL, Sanders CR. Personalized Biochemistry and Biophysics. Biochemistry. 2015; 54:2551–2559. [PubMed: 25856502]
39. Alexov E. Advances in Human Biology: Combining Genetics and Molecular Biophysics to Pave the Way for Personalized Diagnostics and Medicine. Adv Biol. 2014; 2014
40. Kabsch W. Software XDS for image rotation, recognition and crystal symmetry assignment. Acta Crystallogr, Sect D Biol Crystallogr. 2010; 66:125–132. [PubMed: 20124692]
41. Evans PR, Murshudov GN. How good are my data and what is the resolution? Acta Crystallogr D Biol Crystallogr. 2013; 69:1204–14. [PubMed: 23793146]
42. Potterton E, Briggs P, Turkenburg M, Dodson E. A graphical user interface to the CCP 4 program suite. Acta Crystallogr Sect D Biol Crystallogr. 2003; 59:1131–1137. [PubMed: 12832755]
43. Karplus PA, Diederichs K. Linking crystallographic model and data quality. Science (80-). 2012; 336:1030–1033.
44. Weiss MS. Global indicators of X-ray data quality. J Appl Crystallogr. 2001; 34:130–135.
45. Murshudov GN, Skubák P, Lebedev Aa, Pannu NS, Steiner Ra, Nicholls Ra, et al. REFMAC5 for the refinement of macromolecular crystal structures. Acta Crystallogr Sect D Biol Crystallogr. 2011; 67:355–367. [PubMed: 21460454]
46. Adams PD, Afonine PV, Bunkóczi G, Chen VB, Davis IW, Echols N, et al. PHENIX: A comprehensive Python-based system for macromolecular structure solution. Acta Crystallogr Sect D Biol Crystallogr. 2010; 66:213–221. [PubMed: 20124702]
47. Emsley P, Cowtan K. Coot: Model-building tools for molecular graphics. Acta Crystallogr Sect D Biol Crystallogr. 2004; 60:2126–2132. [PubMed: 15572765]
48. Vagin A, Teplyakov A. Molecular replacement with MOLREP. Acta Crystallogr Sect D Biol Crystallogr. 2010; 66:22–25. [PubMed: 20057045]
49. Chen VB, Arendall WB, Headd JJ, Keedy DA, Immormino RM, Kapral GJ, et al. MolProbity: all-atom structure validation for macromolecular crystallography. Acta Crystallogr D Biol Crystallogr. 2010; 66:12–21. [PubMed: 20057044]
50. DeLano, WL. Wwwpymolorg. Version 1. Schrödinger LLC; 2002. The PyMOL Molecular Graphics System.

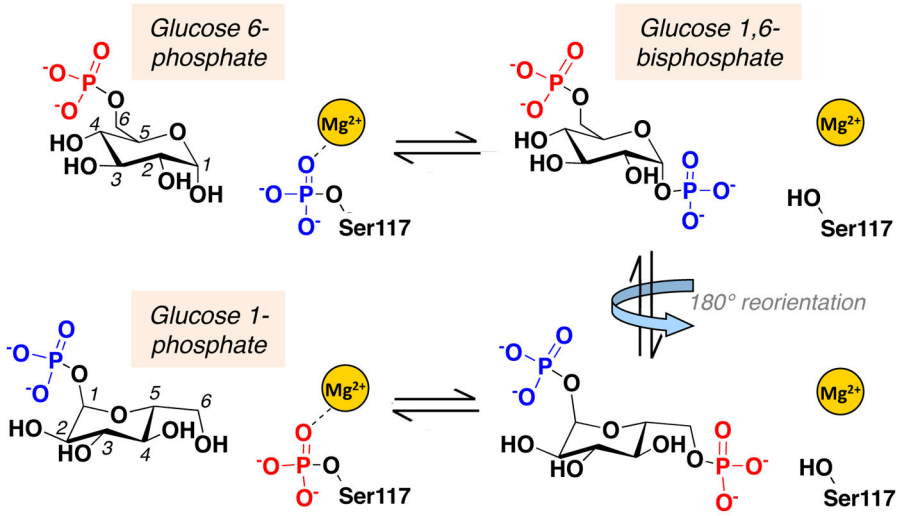

Fig. 1.

A schematic of the catalytic reaction of PGM1, showing the reversible conversion of glucose 6-phosphate to glucose 1-phosphate. The bisphosphorylated intermediate undergoes a 180° reorientation (indicated by blue arrow) in the active site prior to the second phosphoryl transfer.

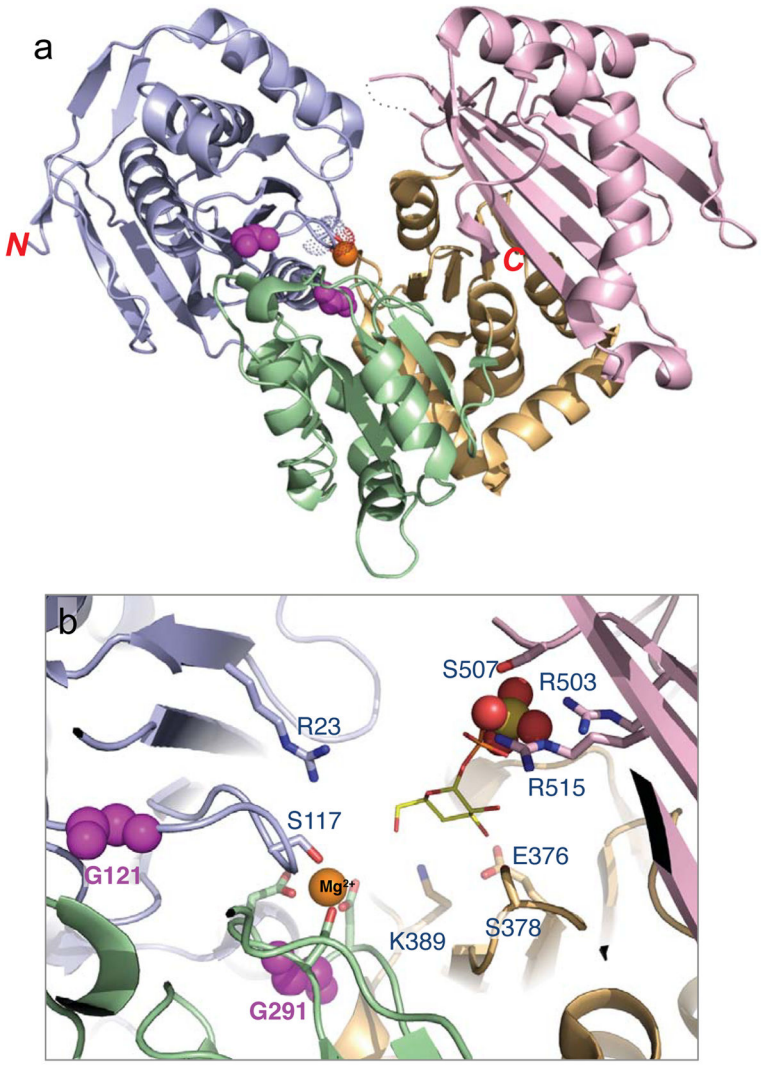

Fig. 2.

The crystal structure of wild-type human PGM1. (a) A ribbon diagram of PGM1 colored by domain. Domain 1 (residues 1–191) is shown in blue, domain 2 (residues 192–304) in green, domain 3 (residues 305–421) in gold, and domain 4 (residues 422–562) in pink. Phosphoserine 117 is highlighted with dots, and Mg^{2+} is shown as an orange sphere. Glycines 121 and 291 are highlighted in magenta. For clarity, the three metal-binding aspartates (residues 288, 290 and 292) are not labeled. Missing residues in the D4 acNve site loop are shown with a doPed line. N- and C-termini are shown with red lePers. (b) A close-up view of the acNve site WT PGM1 showing the four regions (i-iv) discussed in text; side chains of key acNve site residues are shown as sNcks. Colors as in panel (a). The sulfate ion from the crystallizaNon buffer that binds in the phosphate-binding site is shown with spheres. A model for the proposed binding of substrate glucose 1-phosphate is shown in thin lines (yellow), based on a structural superposiNon with a related enzyme-ligand complex (PDB code: 1P5D).

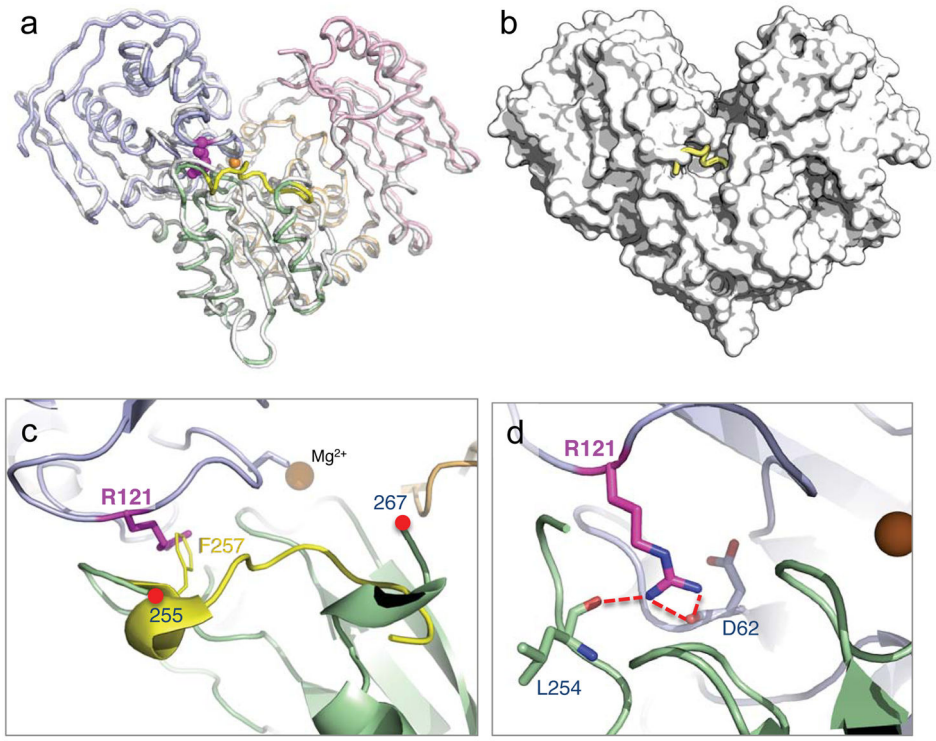

Fig. 3.

Overall structure and detailed views of the G121R crystal structure. (a) A superposiNon of the G121R missense variant (colored by domain as in Fig. 2) and WT PGM1 (white) showing their overall structural similarity. Arg121 is shown in magenta; the region of the WT enzyme corresponding to the disordered residues in the G121R structure is in yellow. (b) The G121R mutant shown with a surface, and superimposed with WT enzyme (yellow), to highlight the patch of disordered residues in the mutant. (c) A close-up view comparing the vicinity of residue 121 in the WT and the G121R structures. The side chain of Phe257 (yellow), which lies in the interface between D1 and D2 in the WT structure, is displaced by Arg121 (magenta), causing disorder from residues 258–264 (between red circles). (d) AdvenNNous hydrogen bonds made between Arg121 and the backbone carbonyl groups of several residues in the D1-D2 interface.

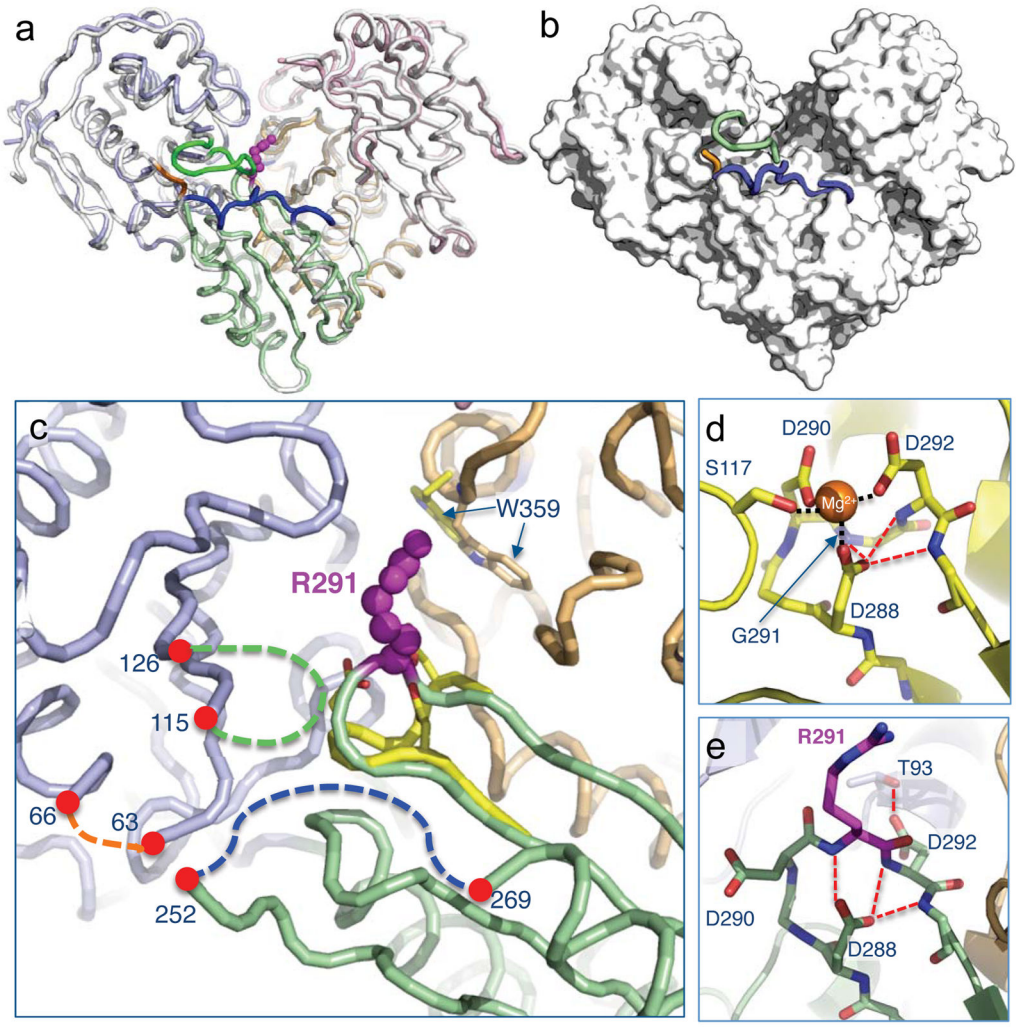

Fig. 4.

Overall and detailed views of the G291R crystal structure. (a) A superposition of the G291R missense variant (colored by domain as in Fig. 2) and WT PGM1 (white) showing their overall structural similarity. Arg291 is shown in magenta; regions of the WT enzyme corresponding to the disordered residues in the mutant structure are highlighted in bright colors: residues 64–65 in orange; residues 116–125 in green; and residues 253–268 in blue. (b) The G291R mutant shown with a surface, and superimposed with WT enzyme as in (a). (c) The vicinity of Arg291 showing its location in the 3-way interface of domains 1, 2, and 3, and locations of the three disordered loops in the mutant structure (dashed lines). The metal binding loop from WT PGM1 is shown in yellow; the position of Trp359 in the WT and G291R structures shows its rearrangement in packing. (d) The metal-binding loop of WT PGM1, showing the bound Mg^{2+} ion, its coordinating aspartates, and location of Ser117. Hydrogen bonds made between Asp288 and other residues in the loop are in dashed red lines; coordinating interactions to the Mg^{2+} ion are in black dotted lines. (e) The region corresponding to (d) in the G291R structure, showing the rearrangement of the three

aspartates and loss of the bound Mg^{2+}. Hydrogen bond interactions of Asp288 and Asp292 are shown with red dashed lines.

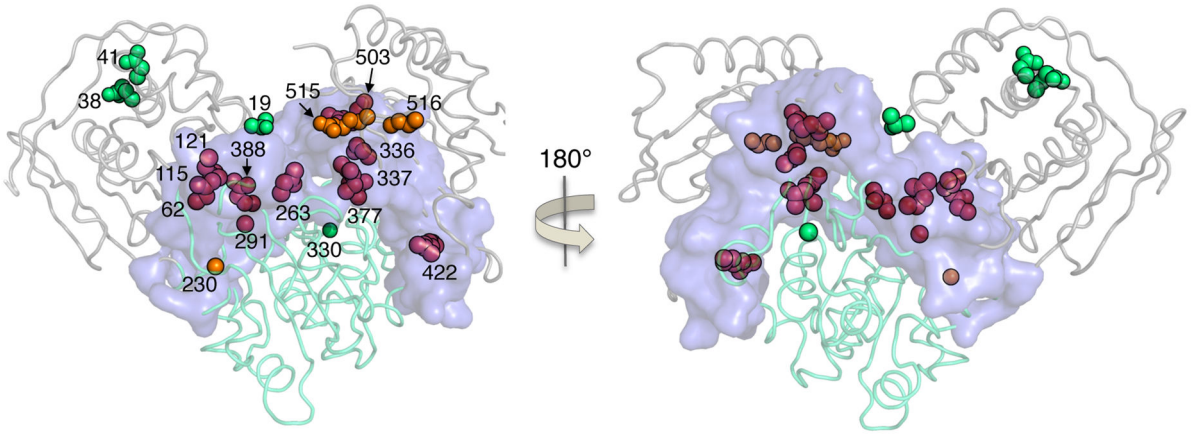

Fig. 5.

Relationship of the known PGM1 missense variants to domain interfaces of the enzyme. A backbone trace of PGM1 showing the interface (blue surface) between the D2/3 unit (cyan) and the rest of the enzyme, i.e., domains 1 and 4 (gray). Most of the known disease-related missense variants cluster in (magenta spheres) or very near (orange spheres) to this extensive interface. The four missense variants that fall outside of this region are shown in green.

Table 1

Data collection and refinement statistics

	WT	G121R	G291R
space group	$P4_12_12$	$P4_12_12$	$P4_12_12$
unit cell parameters (Å)	$a = b$ =172.6, c = 99.8	$a = b$ = 171.4, c = 99.79	$a = b$ = 170.8, c = 99.3
resolution (Å)	61.1–1.75 (1.88–1.85)	54.2 – 2.50 (2.58–2.50)	60.5–2.75 (2.87–2.75)
observations	4273578	740313	544355
unique reflections	162886	51905	38736
$R_{merge}(I)$	0.150 (1.959)	10.5 (1.618)	0.098 (1.566)
$R_{pim}(I)$	0.035 (0.558)	0.041 (0.663)	0.039 (0.640)
Mean $I/\sigma(I)$	18.5 (1.6)	19.6 (1.5)	20.0 (1.6)
Mean $CC_{1/2}$	0.999 (0.885)	0.999 (0.859)	0.999 (0.751)
completeness (%)	100.0 (99.9)	100.0 (99.9)	100.0 (100.0)
multiplicity	33.4 (25.9)	14.3 (13.3)	14.1 (13.4)
no. of protein residues	1118	1066	1063
no. of atoms	9413	8196	7463
no. of SO_4/glycerol molecules	8/9	8/2	5/0
no. of water molecules	819	80	38
R_{cryst}	0.170 (0.309)	0.192 (0.337)	0.210 (0.313)
R_{free}	0.198 (0.351)	0.243 (0.328)	0.271 (0.407)
rmsd bond lengths (Å)	0.007	0.008	0.010
rmsd bond angles (°)	0.998	1.125	1.167
Ramachandran plot [a]			
favored (%)	98.0	95.8	95.2
outliers (residues)	0	6	8
MolProbity score (%-tile)	100	95	99
Average B (Å^2)			
protein	40.0	77.0	80.4
water	44.7	53.0	69.8
coordinate error (Å)[b]	0.19	0.34	0.45
PDB code	5EPC	5F9C	5HSH

Values for the outer resolution shell of data are given in parentheses.

[a] Ramachandran plots generated with Molprobity via the PDB validation server.

[b] Maximum likelihood-based coordinate error estimate reported by PHENIX.

Table 2

Disordered residues and kinetic parameters for the G121R and G291R missense variants relative to WT PGM1.

Protein	Domain of mutation	Disordered residues[a] (no.)	Domain	k_{cat} (s^{-1})	K_m (μM)	% k_{cat} / K_m rel. WT
WT	-	-	-	143±2	80±4	100
G121R	1	258–264 (7)	2	0.368±0.004	56±3	0.4
G291R	2	64–65 (2)	1	b.d.	b.d.	-
		117–125 (9)	1			
		256–267 (12)	2			

[a]Disordered residues are listed relative to WT enzyme as found in chain A of each crystal structure. Kinetic parameters are from [11]; b.d., below detection.